JOURNAL OF THERMOPHYSICS AND HEAT TRANSFER
Vol. 28, No. 3, July–September 2014

Unsteady Internal Forced-Convective Flow Under Dynamic Time-Dependent Boundary Temperature

M. Fakoor-Pakdaman,* Mehran Ahmadi,† and Majid Bahrami‡
Simon Fraser University Surrey, British Columbia V3T 0A3, Canada

DOI: 10.2514/1.T4261

A new all-time analytical model is developed to predict transient internal forced-convection heat transfer under arbitrary time-dependent wall temperature. Slug flow condition is assumed for the velocity profile inside the tube. The solution to the time-dependent energy equation for a step wall temperature is generalized for arbitrary time variations in surface temperature using Duhamel's theorem. A harmonic boundary temperature is considered, and new compact closed-form relationships are proposed to predic: 1) fluid temperature distribution; 2) fluid bulk temperature; 3) wall heat flux; and 4) the Nusselt number. An optimum value is found for the dimensionless angular frequency of the wall temperature to maximize the heat transfer rate of the studied unsteady forced-convective process. Such dimensionless parameter depends upon the imposed-temperature angular frequency, fluid thermophysical properties, and tube geometrical parameters. A general surface temperature is considered, and the temperature field inside the medium is obtained using a superposition technique. An independent numerical simulation is performed using ANSYS® Fluent. The comparison between the obtained numerical data and the present analytical model shows good agreement: a maximum relative difference less than 4.9%.

Nomenclature

A	=	cross-sectional area, Eq. (13), m^2
a	=	half-width of spacing between parallel plates, or circular tube radius, m
c_p	=	heat capacity, $J/kg \cdot K$
Fo	=	Fourier number; $\alpha t/a^2$
J	=	Bessel function, Eq. (6a)
k	=	thermal conductivity, $W/m \cdot K$
Nu	=	Nusselt number, ha/K
n	=	positive integer, Eq. (6b)
p	=	0 for parallel plate and 1 for circular tube, Eqs. (3) and (14)
Pr	=	Prandtl number (ν/α)
q_w^*	=	dimensionless wall heat flux
Re	=	Reynolds number, $2Ua/\nu$
r	=	radial coordinate measured from circular tube centerline, m
T	=	temperature, K
U	=	velocity magnitude, m/s
$\boldsymbol{u}$	=	velocity vector, Eq. (2)
x	=	axial distance from the entrance of the heated section, m
y	=	normal coordinate measured from centerline of parallel plate channel, m
α	=	thermal diffusivity, m^2/s
γ	=	function for circular tube [Eq. (6a)] or for parallel plate [Eq. (6b)]
$\Delta\varphi$	=	thermal lag (phase shift)
ζ	=	dummy X variable
η	=	dimensionless radial/normal coordinate for circular tube equal to r/a or for parallel plate equal to y/a
θ	=	dimensionless temperature; $(T - T_0)/\Delta T_R$
λ_n	=	eigenvalues, Eq. (6)
ν	=	kinematic viscosity, m^2/s
ξ	=	dummy Fo variable
ρ	=	fluid density, kg/m^3
ψ	=	arbitrary function of Fo
Ω	=	imposed-temperature angular frequency, rad/s
ω	=	dimensionless temperature angular frequency,

Subscripts

m	=	mean or bulk value
R	=	reference value
s	=	step wall (surface) temperature
w	=	wall
0	=	inlet

Received 23 August 2013; revision received 23 November 2013; accepted for publication 9 January 2014; published online 21 April 2014.

*Laboratory for Alternative Energy Convection, School of Mechatronic Systems Engineering, No. 4300, 250-13450 102nd Avenue; mfakoorp@sfu.ca.

†Laboratory for Alternative Energy Convection.

‡Laboratory for Alternative Energy Convection; mbahrami@sfu.ca.

I. Introduction

DEVELOPING an in-depth understanding of unsteady forced-convection heat transfer is crucial for optimal design and accurate control of heat transfer in emerging sustainable energy applications and next-generation heat exchangers. The origin of thermal transients in sustainable energy applications include the variable thermal load on 1) thermal solar panels in thermal energy storage (TES) systems [1–3]; 2) power electronics of solar/wind/tidal energy conversion systems [4,5]; and 3) power electronics and electric motor (PEEM) of hybrid electric vehicles (HEVs), electric vehicles (EVs), and fuel cell vehicles (FCVs) [6–9].

Solar thermal systems are widely used in solar powerplants and are being widely commercialized. Solar powerplants have seen about 740 MW of generating capacity added between 2007 and the end of 2010, bringing the global total to 1095 MW [5]. Such growth is expected to continue, as in the United States at least another 6.2 GW capacity is expected to be in operation by the end of 2013 [5]. However, the growth of such technology is hindered by the inherent variability of solar energy subjected to daily variation, seasonal variation, and weather conditions [1,4,10]. To overcome the issue of the intermittency, TES systems are used to collect thermal energy to smooth out the output and shift its delivery to a later time. Single-phase sensible heating systems or latent heat storage systems using phase change materials are used in TES; transient heat exchange occurs to charge or discharge the storage material [11]. From the technical point of view, one of the main challenges facing TES systems is designing suitable heat exchangers to work reliably under unsteady conditions [11]: a key issue that this research attempts to address.

To assure reliable performance of electronic components, the temperature of different components should be maintained below

recommended values. The temperature of power electronics can vary significantly with the fluid flow and the applied heat flux over time [12]. Thus, it is important to investigate the transient thermal behavior of these systems, especially during peak conditions [13]. Furthermore, new application of transient forced convection has emerged by the advent of HEVs, EVs, and FCVs. Since introduced, the sales of such vehicles have grown at an average rate of more than 80% per year. As of October 2012, more than 5.8 million HEVs have been sold worldwide since their inception in 1997 [14]. Their hybrid powertrain and power electronics electric motors undergo a dynamic thermal load as a direct result of driving/duty cycle and environmental conditions. Conventional cooling systems are designed based on a nominal steady state, typically a worst-case scenario [15], which may not properly represent the thermal behavior of various applications or duty cycles. This clearly indicates the enormity of the pending need for in-depth understanding of the instantaneous thermal characteristics of the aforementioned thermal systems [16]. Successful and intelligent thermal design of such dynamic systems leads to the design of new efficient heat exchangers to enhance the overall efficiency and reliability of TES and PEEM cooling solutions, which in the cases of the HEVs/EVs/FCVs means significant improvement in vehicle efficiency/reliability and fuel consumption [15–18].

In all the aforementioned applications, transient heat transfer occurs in heat exchangers subjected to arbitrary time-dependent duct wall temperature. This phenomenon can be represented by an unsteady forced-convective tube flow, which is the ultimate goal of this study.

Siegel pioneered the study of transient internal forced convection by investigating a duct flow following a step change in wall heat flux or temperature [19,20]. Later, Sparrow and Siegel [21,22] used an integral technique to analyze transient heat transfer in the thermal entrance region of a Poiseuille flow under step wall temperature/heat flux. Moreover, the tube wall temperature of channel flows for particular types of position/time-dependent heat fluxes was studied in the literature [23–27]. A number of studies were conducted on effects of periodic inlet temperature on the heat transfer characteristics of a convective tube flow under step wall temperature [28–33]. Most studies on unsteady internal forced convection are limited to homogeneous/constant boundary conditions at the tube wall, i.e., isothermal or isoflux; a summary of the available studies is presented in Table 1.

Our literature review indicates the following:

1) The effects of periodic/arbitrary time-dependent surface temperatures on thermal performance of an internal forced-convective flow have not been investigated.

2) There is no model to predict the fluid temperature distribution, wall heat flux, and the Nusselt number of a tube flow under arbitrary time-dependent surface temperatures.

3) No study has been conducted to determine the optimum conditions that maximize the convective heat transfer rate in tube flows under harmonic boundary conditions.

4) The parameters, including temperature amplitude, angular frequency, and fluid thermal lag (phase shift), affecting the unsteady internal forced convection have not been presented in the literature.

In previous work [34,35], a comprehensive study was carried out on the thermal characteristics of a convective tube flow under dynamically varying heat flux. In the present study, a new analytical all-time model is developed in Cartesian and cylindrical coordinates to accurately predict 1) fluid temperature distribution; 2) fluid bulk temperature; 3) wall heat flux; and 4) the Nusselt number, for a tube flow under arbitrary time-dependent temperature. New dimensionless variables are introduced that characterize transient forced convection inside a conduit under a time-dependent boundary temperature. An optimum condition is presented that maximizes the heat transfer rate of internal forced convection under a harmonic boundary temperature. The present paper provides new insight on unsteady heat transfer, and it serves as a platform and an engineering tool to investigate and develop intelligent transient thermal systems for a wide variety of engineering applications.

To develop the present analytical model, the fluid flow response for a step surface temperature is taken into account. Using Duhamel's theorem [36], the thermal characteristics of the fluid flow are determined analytically under a periodic time-dependent surface temperature. New dimensionless variables are introduced, and the system is optimized to maximize the heat transfer rate under harmonic boundary temperature. Any type of time-dependent surface temperature can be decomposed into sinusoidal functions using a sine Fourier series transformation [36]. Thus, the present model for the harmonic excitation is applied to find the temperature distribution of a tube flow under a general time-dependent boundary condition.

II. Governing Equations

Figure 1 shows a laminar forced-convective internal flow inside a parallel plate or a circular tube. The tube is thermally insulated in the first subregion, $x \leq 0$, and at $t = 0$; the second subregion of tube wall at $x \geq 0$ is instantaneously subjected to an arbitrary time-dependent temperature, $T_w = \varphi(t)$. The tube and fluid are assumed to be initially isothermal at initial temperature T_0. The entering fluid temperature is also maintained at T_0 throughout the heating period. The tube is assumed long enough so that it covers both thermally developing and fully developed regions; see Fig. 1. It is intended to determine the evolution of the fluid temperature, wall heat flux, and the Nusselt number as a function of time and space for the entire range of the Fourier number under arbitrary time-dependent wall temperature.

The assumptions made in deriving the mathematical model of the proposed unsteady heat convection process are 1) laminar incompressible flow; 2) negligible tube wall thermal inertia; 3) constant thermophysical properties; negligible viscous dissipation; negligible axial heat conduction, i.e., $Pe = Re \times Pr > 10$ [37]; 4) no thermal energy sources within the fluid; and 5) uniform velocity profile along the tube, i.e., slug flow.

Slug flow assumption can predict the thermal behavior of any type of fluid flow close to the tube entrance where the velocity profile is developing and has not reached the fully developed condition [24].

As such, the energy equation for a fluid flowing inside a duct in vectorial notation in this at any instance is shown by Eq. (1):

$$\frac{\partial T}{\partial t} + \boldsymbol{u} \cdot \nabla T = \alpha \cdot \nabla^2 T \tag{1}$$

where $\boldsymbol{u}$ and α are the velocity and the thermal diffusivity of the fluid, respectively. For the case of slug flow, the flow is considered one-dimensional and fluid velocity inside the duct is considered constant, as indicated by Eq. (2):

$$\boldsymbol{u} = U\hat{\boldsymbol{i}}, \qquad U = \text{const} \tag{2}$$

Accordingly, the dimensionless energy equation in Cartesian and cylindrical coordinates can be written in a unified form as follows:

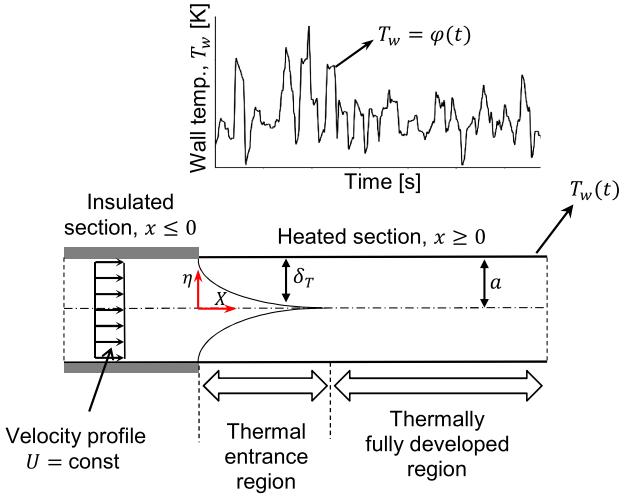

Fig. 1 Schematic of laminar forced-convective tube flow under arbitrary time-dependent wall temperature inside a parallel plate or a circular tube.

$$\frac{\partial\theta}{\partial Fo}+\frac{\partial\theta}{\partial X}=\frac{1}{\eta^p}\frac{\partial}{\partial\eta}\left(\eta^p\frac{\partial\theta}{\partial\eta}\right) \tag{3}$$

It should be noted that superscript p takes the values of 0 and 1, respectively, for Cartesian and cylindrical coordinates. In fact, the former is attributed to the fluid flow between parallel plates, and the latter indicates the fluid flow inside a circular tube. The dimensionless variables are

$$\theta=\frac{T-T_0}{\Delta T_R},\qquad Fo=\frac{\alpha t}{a^2},\qquad X=\frac{2\frac{x}{a}}{Re\cdot Pr},$$
$$Re_a=\frac{2Ua}{\upsilon},\qquad Pr=\frac{\upsilon}{\alpha},\qquad Nu_a=\frac{ha}{k}$$

where ΔT_R is the amplitude of the imposed temperature, Fo is the Fourier number, and X is the dimensionless axial position. In addition, for parallel plate and circular tube, $\eta=\frac{y}{a}$ and $\eta=\frac{r}{a}$, respectively.

Equation (4) is subjected to the following boundary and initial conditions:

$$\theta(0,\eta,Fo)=0 \quad \text{at } X=0, \qquad Fo>0, \qquad 0\le\eta\le 1 \tag{4a}$$

$$\frac{\partial\theta(X,0,Fo)}{\partial\eta}=0 \quad \text{at } \eta=0, \qquad X>0, \qquad Fo>0 \tag{4b}$$

$$\theta(X,1,Fo)=\psi(Fo) \quad \text{at } \eta=1, \qquad X>0, \qquad Fo>0 \tag{4c}$$

$$\theta(X,\eta,0)=0 \quad \text{at } Fo=0, \qquad X>0, \qquad 0\le\eta\le 1 \tag{4d}$$

where $\psi(Fo)$ is an arbitrary time-dependent temperature imposed on the tube wall.

III. Model Development

In this section, a new all-time model is developed in Cartesian and cylindrical coordinates, considering 1) short-time response; and 2) long-time response. As such, the presented model predicts the temperature distribution inside a convective tube flow under an arbitrary time-dependent temperature imposed on the tube wall.

For a duct flow at uniform temperature T_0, instantaneously subjected to a step surface temperature, the temperature response is given in [19]:

$$\theta_s=\frac{T_w-T_0}{\Delta T_R}\left[1-2\sum_{n=1}^{\infty}\gamma_n(\eta)\exp(-\lambda_n^2 Fo)\right] \tag{5}$$

1) In cylindrical coordinate, i.e., flow inside a circular tube,

$$\gamma_n(\eta)=\frac{J_0(\lambda_n\eta)}{\lambda_n J_1(\lambda_n)}, \quad \text{and} \quad J_0(\lambda_n)=0, \qquad \lambda_n>0 \tag{6a}$$

2) In Cartesian coordinate, i.e., flow between parallel plates,

$$\gamma_n(\eta)=\frac{(-1)^{n-1}}{\lambda_n}\cos(\lambda_n\eta), \text{ and } \lambda_n=\frac{2n-1}{2}\pi, \quad n=1,2,3,\ldots \tag{6b}$$

where θ_s is the dimensionless temperature of the fluid under step wall temperature. J_0 and J_1 are the zero- and first-order Bessel functions of the first kind, and λ_n are the eigenvalues in cylindrical or Cartesian coordinates: Eqs. (6a) and (6b), respectively. The energy equation for a tube flow is linear; Eq. (4). This shows the applicability of a superposition technique to extend the response of the fluid flow for a step surface temperature to the other general cases, as discussed in [25]. As such, byusing Duhamel's theorem [36], the thermal response for a step surface temperature [Eq. (6)] can be generalized for an arbitrary time variation in surface temperature [Eq. (4c)]:

$$\theta=\frac{T-T_0}{\Delta T_R}=2\sum_{n=1}^{\infty}\lambda_n^2\gamma(\eta)\exp(-\lambda_n^2 Fo)\times\int_0^{Fo}\psi(\xi)\exp(\lambda_n^2\xi)\,\mathrm{d}\xi \tag{7}$$

This expression is valid only if the element is initially isothermal, so the solution here is limited to the cases where the channel is initially isothermal. However, the extension to the other cases, e.g., when the fluid initially has a steady state temperature distribution, can be obtained by superposition techniques, as discussed in [25].

As shown in Fig. 2, in an Eulerian coordinate system, the observer is fixed at a given location x along the tube and the fluid moves by. It will take some time, $t=x/U$, $Fo=X$, for the entrance fluid to reach the axial position X. Beyond this region, i.e., $X\ge Fo$, where the inlet fluid will not have enough time to penetrate, convection heat transfer plays no role; hence, the conduction becomes the dominant mechanism for transferring heat from the wall to the fluid. The behavior in this region is similar to a tube with infinite length in both directions. This means that the convective term in the energy equation [Eq. (1)] drops and a pure transient "heat-conduction" process takes place. On the other hand, for $X<Fo$, the observer situated at axial position X feels the passing fluid that has had enough time to reach from the insulated entrance section. This region is considered as the long-time response of the fluid flow [25]. Therefore, the solution consists of two regions that should be considered separately. The methodology considered in this study is shown schematically in Fig. 2.

A. Short-Time Response, $X\ge Fo$

For the sake of generality, we consider a case in which the surface temperature varies with both time and space, $\psi(X,Fo)$. We first consider the region where $X\ge Fo$. A fluid element that reaches X at time Fo was already in the heated section at the location $X-Fo$ at the beginning of the transient. As this element moves along, it is subjected to the surface temperature variations in both time and space. At a time ξ between 0 and Fo, the element is arrived to the location $X-Fo+\xi$. Thus, the tube wall temperature that the element is subjected to at that time is $\psi(X-Fo+\xi,\xi)$. This is substituted into Eq. (7) to find the short-time response for the fluid temperature distribution inside a circular tube and parallel plate, respectively [24]:

$$\theta(X,\eta,Fo)=\frac{T-T_0}{\Delta T_R}=2\sum_{n=1}^{\infty}\lambda_n^2\gamma_n(\eta)\exp(-\lambda_n^2 Fo)$$
$$\times\int_0^{Fo}\psi(X-Fo+\xi,\xi)\exp(\lambda_n^2\xi)\,\mathrm{d}\xi \tag{8}$$

It should be noted that, according to Eq. (8), when the imposed tube wall temperature is only a function of time $\psi=\psi(Fo)$, the short-time thermal response of the fluid flow is not dependent upon the

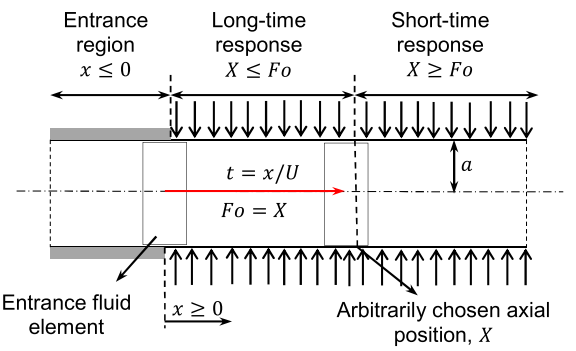

Fig. 2 Schematic of the two main regions adopted to find the transient thermal response of the tube flow.

axial position. However, it is a function of time and the characteristics of the imposed surface temperature.

B. Transition Time, $X = Fo$

For each axial position, the short-time and long-time responses are equal at $X = Fo$. This is the dimensionless transition time for a given axial position. Therefore, the time $Fo = X$ can be considered a demarcation between the short-time and long-time responses for each axial position. For instance, for an arbitrarily-chosen axial position $X = 1.2$, the dimensionless transition time is $Fo = 1.2$.

C. Long-Time Response, $X < Fo$

Now, we consider the region where $X < Fo$. The element that reaches X at time Fo has entered the channel at the time $Fo - X$ and begun to be heated. As time elapses from when the transition begins, this element will reach the location ζ at the time $Fo - X + \zeta$. Thus, the surface temperature that the element is subjected to at that location is $\psi(\zeta, Fo - X + \zeta)$. Substituting this into Eq. (7) results in Eq. (9), which represents the long-time response of the flow inside a circular tube or a parallel plate [24]:

$$\theta(X,\eta,Fo) = \frac{T - T_0}{\Delta T_R} = 2\sum_{n=1}^{\infty} \lambda_n^2 \gamma_n(\eta) \exp(-\lambda_n^2 Fo) \times \int_0^{Fo} \psi(\zeta, Fo - X + \zeta) \exp(\lambda_n^2 \xi)\, d\xi \tag{9}$$

According to Eq. (9), the long-time thermal response of the fluid flow is a function of time, axial position, and characteristics of the imposed tube wall temperature.

IV. Harmonic Thermal Transients

In this section, thermal response of a tube flow is obtained under a harmonic wall temperature, prescribed as follows:

$$T_w = T_0 + \Delta T_R[1 + \sin(\Omega t)] \tag{10}$$

where ΔT_R K and Ω rad/s are the amplitude and the angular frequency of the imposed wall temperature. The analytical model is presented in form of 1) closed-form series solutions; and 2) approximate compact easy-to-use relationships.

Any type of prescribed time-dependent wall temperature can be decomposed into simple oscillatory functions using a Fourier series transformation [36]. Using a superposition technique, the results can be extended to the cases with an arbitrary time-dependent wall temperature as a general boundary condition; see Sec. IV.H.

A. Exact Series Solutions

The dimensionless form of Eq. (10) is as follows:

$$\theta_w(\omega, Fo) = \frac{T_w - T_0}{\Delta T_R} = 1 + \sin(\omega Fo) \tag{11}$$

where $\omega = \Omega a^2/\alpha$ is the dimensionless angular frequency. Substituting Eq. (11) into Eqs. (8) and (9), after some algebraic manipulations, the short-time and long-time temperature distributions inside the fluid are obtained. In this study, we considered the first 60 terms of the series solutions; using more terms does not affect the results up to four decimal digits.

1) Short-time fluid temperature distribution, $X \geq Fo$,

$$\theta(\omega,\eta,Fo) = 1 + \sin(\omega Fo) + 2\sum_{n=1}^{\infty} \gamma_n(\eta) \times \left\{ \frac{[\omega\lambda_n^2 - (\omega^2 + \lambda_n^4)]\exp(-\lambda_n^2 Fo) - \omega^2 \sin(\omega Fo) - \omega\lambda_n^2 \cos(\omega Fo)}{\omega^2 + \lambda_n^4} \right\} \tag{12a}$$

2) Long-time fluid temperature distribution, $X \leq Fo$,

$$\theta(\omega,X,\eta,Fo) = 1 + \sin(\omega Fo) + 2\sum_{n=1}^{\infty} \gamma_n(\eta) \times \left\{ \frac{-\lambda_n^2\omega\cos(\omega Fo) - \omega^2 \sin(\omega Fo)}{\omega^2 + \lambda_n^4} - \frac{\{\lambda_n^4 \sin[\omega(Fo - X)] - \lambda_n^2\omega \cos[\omega(Fo - X)] - (\omega^2 + \lambda_n^4)\} \times \exp(-\lambda_n^2 X)}{\omega^2 + \lambda_n^4} \right\} \tag{12b}$$

It should be noted that the definition of $\gamma_n(\eta)$ and the eigenvalues λ_n have been previously given by Eqs. (6a) and (6b) for a circular tube and a parallel plate, respectively. In addition, the fluid bulk temperature can be obtained by Eq. (13) [38]:

$$\theta_m(\omega, X, Fo) = \frac{1}{A}\iint_A \theta\, dA \tag{13}$$

where A is the cross-sectional area of the tube at any arbitrary axial position. After performing the integration in Eq. (13), the following relationships are obtained to evaluate the fluid bulk temperature.

Short-time dimensionless fluid bulk temperature, $X \geq Fo$,

$$\theta_m(\omega, Fo) = 1 + \sin(\omega Fo) + 2^p \sum_{n=1}^{\infty} \times \frac{[\omega\lambda_n^2 - (\omega^2 + \lambda_n^4)]\exp(-\lambda_n^2 Fo) - \omega^2 \sin(\omega Fo)\omega\lambda_n^2 \cos(\omega Fo)}{\lambda_n^2(\omega^2 + \lambda_n^4)} \tag{14a}$$

Long-time dimensionless fluid bulk temperature, $X \leq Fo$,

$$\theta_m(\omega, X, Fo) = 1 + \sin(\omega Fo) + 2^p \sum_{n=1}^{\infty} \left\{ \frac{-\lambda_n^2\omega \cos(\omega Fo) - \omega^2 \sin(\omega Fo)}{\lambda_n^2(\omega^2 + \lambda_n^4)} - \frac{\{\lambda_n^4 \sin[\omega(Fo - X)] + \lambda_n^2\omega \cos[\omega(Fo - X)] - (\omega^2 + \lambda_n^4)\} \times \exp(-\lambda_n^2 X)}{\lambda_n^2(\omega^2 + \lambda_n^4)} \right\} \tag{14b}$$

The eigenvalues λ_n for the fluid flow inside a circular tube and a parallel plate can be obtained by Eqs. (6a) and (6b), respectively.

The dimensionless heat flux at the tube wall can be evaluated by

$$q_w^* = \left.\frac{\partial\theta}{\partial\eta}\right|_{\eta=1} \tag{15}$$

Differentiating the fluid temperature [Eqs. (12a) and (12b)] at the tube wall, we obtain the following:

Short-time dimensionless wall heat flux, $X \geq Fo$,

$$q_w^*(\omega, Fo) = -2\sum_{n=1}^{\infty} \times \frac{[\omega\lambda_n^2 - (\omega^2 + \lambda_n^4)]\exp(-\lambda_n^2 Fo) - \omega^2 \sin(\omega Fo) - \omega\lambda_n^2 \cos(\omega Fo)}{\omega^2 + \lambda_n^4} \tag{16a}$$

Long-time dimensionless wall heat flux, $X \leq Fo$,

$$q_w^*(\omega, X, Fo) = -2\sum_{n=1}^{\infty} \times \frac{\omega\lambda_n^2 \sin(\omega Fo) - \omega^2 \cos(\omega Fo) - \{\lambda_n^4 \cos[\omega(Fo - X)] + \lambda_n^2\omega \sin[\omega(Fo - X)]\} \times \exp(-\lambda_n^2 X)}{\omega^2 + \lambda_n^4} \tag{16b}$$

In this study, the local Nusselt number is defined based on the difference between the tube wall and fluid bulk temperatures; see Bejan [39]:

$$Nu_a(\omega, X, Fo) = \frac{ha}{k} = \frac{q_w^*}{\theta_w - \theta_m} = \frac{q_w^*}{[1 + \sin(\omega Fo)] - \theta_m} \tag{17}$$

It should be noted that the characteristics length α for the Nusselt number is the half-width of a parallel plate in the Cartesian coordinate and the tube radius in the cylindrical coordinate. Therefore, the short-time Nusselt number can be obtained by substituting Eqs. (14a) and (14b) into Eq. (17); similarly, substituting Eqs. (16a) and (16b) into Eq. (17) indicates the long-time Nusselt number.

To optimize the transient internal forced convection, we define a new parameter, the average dimensionless wall heat flux, as follows:

$$\bar{q}_w^*(\omega) = \frac{1}{Fo \times X}\int_{\xi=0}^{Fo}\int_{\zeta=0}^{X} q_w^* \, \mathrm{d}\zeta \, \mathrm{d}\xi \tag{18}$$

where Fo is the Fourier number (dimensionless time), and X is an arbitrarily chosen axial position. Equation (18) shows the average heat transfer rate over an arbitrary period of time Fo and length of the tube X. This will be discussed in more detail in Sec. VI.

B. Approximate Compact Relationships

Since using the series solutions presented in Section IV.E is tedious, the following new compact easy-to-use relationships are proposed to predict 1) dimensionless fluid bulk temperature; 2) dimensionless wall heat flux; and 3) Nusselt number, for fluid flow inside a parallel plate. As such, the MATLAB curve fitting tool was used to find the proposed compact relationships. Therefore, analytical results for different dimensionless numbers were curve fitted to find the most appropriate form of the compact relationships with minimum relative difference compared to the obtained series solutions. The proposed compact relationships are compared with the exact series solutions in graphical form in Sec. VI.

1. Dimensionless Fluid Bulk Temperature

For $\omega \geq \pi$, the following compact relationships predict the exact series solutions for the fluid bulk temperature [Eqs. (14a) and (14b)] by the maximum relative difference less than 9.1%.

1) Compact short-time fluid bulk temperature, $X \geq Fo$,

$$\theta_m(\omega, Fo) = \frac{1.078 \times Fo}{Fo + 0.1951} + \left(\frac{1.616}{\omega + 1.023}\right) \times \exp\left(-\frac{0.3748 \times \omega + 28.78}{\omega + 9.796} \times Fo\right) + \frac{0.0934 \times \omega + 2.86}{\omega + 1.802} \times \sin\left(\omega Fo + \frac{-0.78\omega^2 + 17.8 \times \omega - 160.9}{\omega^2 - 22.3 \times \omega + 200.7}\right) \tag{19a}$$

2) Compact long-time fluid bulk temperature, $X \leq Fo$,

$$\theta_m(\omega, X, Fo) = \frac{1.078 \times X}{X + 0.1951} + \frac{0.1167 \times \omega + 3.575}{\omega + 1.802} \times \sin\left(\omega Fo + \frac{-0.78\omega^2 + 17.8 \times \omega - 160.9}{\omega^2 - 22.3 \times \omega + 200.7}\right) \tag{19b}$$

2. Dimensionless Wall Heat Flux

For $Fo \geq 0.05$ and $\omega \geq \pi$, the dimensionless wall heat flux can be obtained by the following compact relationships. The maximum relative difference between the developed compact relationships [Eqs. (20a) and (20b)] and the exact series solutions [Eqs. (16a), (16b)] is less than 5.1%.

1) Compact short-time wall heat flux, $X \geq Fo$,

$$q_w^*(\omega, Fo) = \frac{-0.206 \times Fo + 0.449}{Fo + 0.132} + \frac{14.73 \times \omega + 103.2}{\omega + 70.74} \times \sin\left(\omega Fo + \frac{-0.77\omega^2 - 23.45 \times \omega + 215.3}{\omega^2 - 30.51 \times \omega + 280.5}\right) \tag{20a}$$

2) Compact long-time wall heat flux, $X \leq Fo$,

$$q_w^*(\omega, X, Fo) = 3.037 \times \exp(-4.626X) + \frac{-0.206 \times X + 0.449}{X + 0.132} + \frac{14.73 \times \omega + 103.2}{\omega + 70.74} \times \sin\left(\omega Fo + \frac{-0.77\omega^2 - 23.45 \times \omega + 215.3}{\omega^2 - 30.51 \times \omega + 280.5}\right) \tag{20b}$$

3. Nusselt Number

Using the definition of the Nusselt number [Eq. (17)], a compact closed-form relationship can also be obtained for Nusselt number. The short-time Nusselt number can be developed by substituting

Eqs. (17a) and (20a) into Eq. (17). Similarly, the long-time Nusselt number can be obtained by substituting Eqs. (19b) and (20b) into Eq. (17).

We believe that the form of the compact relationships presented in this section reveals the nature of the transient problem herein under consideration. This will be discussed in detail in Sec. VI.

V. Numerical Study

To verify the presented analytical solution, an independent numerical simulation of the planar flow inside a parallel plate is performed using the commercial software ANSYS® Fluent. User-defined codes are written to apply the harmonic and arbitrary time-dependent temperatures on the tube wall: Eqs. (10) and (22), respectively. Model geometry and boundary conditions are similar to what is shown in Fig. 1. Furthermore, the assumptions stated in Sec. II are used in the numerical analysis; however, the fluid axial conduction is not neglected in the numerical analysis. Grid independency of the results is tested for three different grid sizes: 20×100 and 40×200, as well as 80×400. Finally, 40×200 is selected as the final grid size, since the maximum difference in the predicted values for the fluid temperature by the two latter grid sizes is less than 1%. The geometrical and thermal properties used in the baseline case for the numerical simulation are listed in Table 2. The maximum relative difference between the analytical results and the numerical data is less than 4.9%, which is discussed in detail in Sec. VI.

VI. Results and Discussion

A. Harmonic Prescribed Temperature

Although the methodology developed in Sec. III is presented for Cartesian and cylindrical coordinates, only the results for the former are discussed in this section in a graphical form. The trends for the cylindrical coordinate are similar.

Variations of the dimensionless centerline temperature against the Fo number [Eqs. (12a) and (12b)] for a few axial positions along the tube are shown in Fig. 3 and compared with the numerical data obtained in Sec. V. Periodic temperature is imposed on the tube wall; Eq. (11). The solid lines in Fig. 3 represent our analytical results, and the markers show the obtained numerical data. There is an excellent agreement between the analytical results [Eqs. (12a) and (12b)] and the obtained numerical data, with a maximum relative difference less than 4.9%.

The following is shown in Fig. 3:

1) The present model predicts an abrupt transition between the short-time and long-time responses. The numerical results, however, indicate a smooth transition. This causes the numerical data to deviate slightly from the analytical results as the long-time response begins. Such transitions are demarcated by dashed lines on the figure.

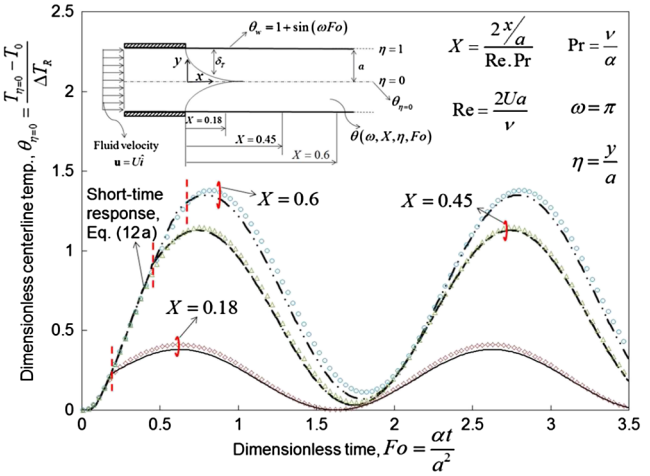

Fig. 3 Variations of centerline temperature versus the dimensionless time (Fourier number) for different axial positions [Eqs. (12a) and (12b)] and comparison with the obtained numerical data (markers).

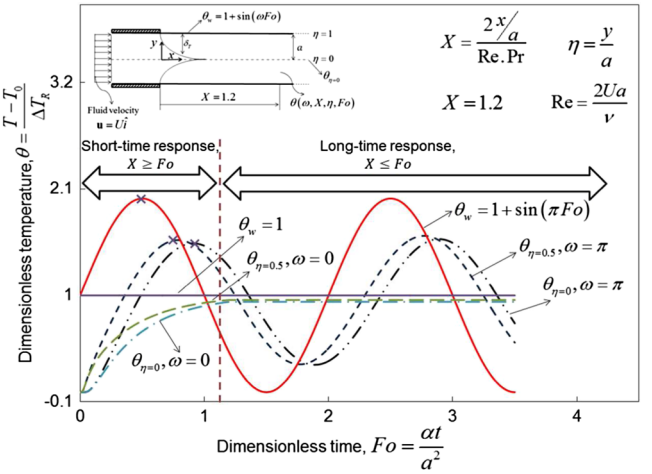

Fig. 4 Dimensionless fluid temperature against Fo number for cyclic and step heat fluxes.

2) The abrupt transition from short-time to long-time responses is attributed to the analytical method that Siegel [19] used to solve the transient energy equation for a step wall temperature. This is discussed in detail in [19].

3) There is an initial transient period of "pure conduction" during which all the curves follow along the same line, $X \geq Fo$; Eq. (12a).

4) When $Fo = X$, each curve moves away from the common line, i.e., pure conduction response, and adjusts toward a steady oscillatory behavior at a long-time response; Eq. (12b). The wall temperatures increase for larger X values, as expected; this is due to the increase of the fluid energy (bulk temperature) along the axial direction.

5) Increasing length-to-diameter ratio increases the axial position number, which in turn increases the temperature inside the fluid.

6) The higher the velocity inside the tube, the higher the Re number, which in turn decreases the axial position number, $X = (2x/a)/(Re_a \cdot Pr)$ and leads to lower temperature inside the fluid.

Figure 4 shows the variations of the dimensionless fluid temperature at different radial positions across the tube versus the Fo number; Eqs. (12a) and (12b). Harmonic and step temperatures are imposed at the tube wall, i.e., $\theta_w = 1 + \sin(\pi Fo)$ and $\theta_w = 1$, respectively. As such, the short-time and long-time fluid temperatures at different radial positions at an arbitrarily chosen axial position, $X = 1.2$, are obtained using Eqs. (12a) and (12b).

From Fig. 4, the following conclusions can be drawn:

1) As expected at any given axial position, the fluid temperature oscillates with time in the case of a prescribed harmonic wall temperature. For a step surface temperature, $\omega = 0$, the solution does not fluctuate over time.

2) At any given axial position, there is an initial transient period, which can be considered as pure conduction, i.e., the short-time response for $X \geq Fo$. However, as pointed out earlier, each axial position shows steady oscillatory behavior for $X \leq Fo$ at the long-time response. Therefore, for the arbitrarily chosen axial position of $X = 1.2$, the long-time response begins at $Fo = 1.2$ and shows the same behavior all-time thereafter.

3) For an imposed cyclic wall temperature, the fluid temperature oscillates around the associated response for the step surface temperature with the same angular frequency at which the system is excited.

4) The shift between the peaks of the temperature profile is marked at different radial positions. This shows a "thermal lag" (phase shift) of the fluid flow, which increases toward the centerline of the tube. This thermal lag is attributed to the fluid thermal inertia.

Figure 5 shows the variations of the dimensionless centerline temperature at a given axial position of $X = 1.2$ versus the Fourier number and the angular frequency; Eqs. (12a) and (12b).

The following can be concluded from Fig. 5:

1) At the two limiting cases where 1) $\omega \to 0$ and 2) $\omega \to \infty$, the fluid flow response yields that of a step surface temperature (isothermal boundary condition).

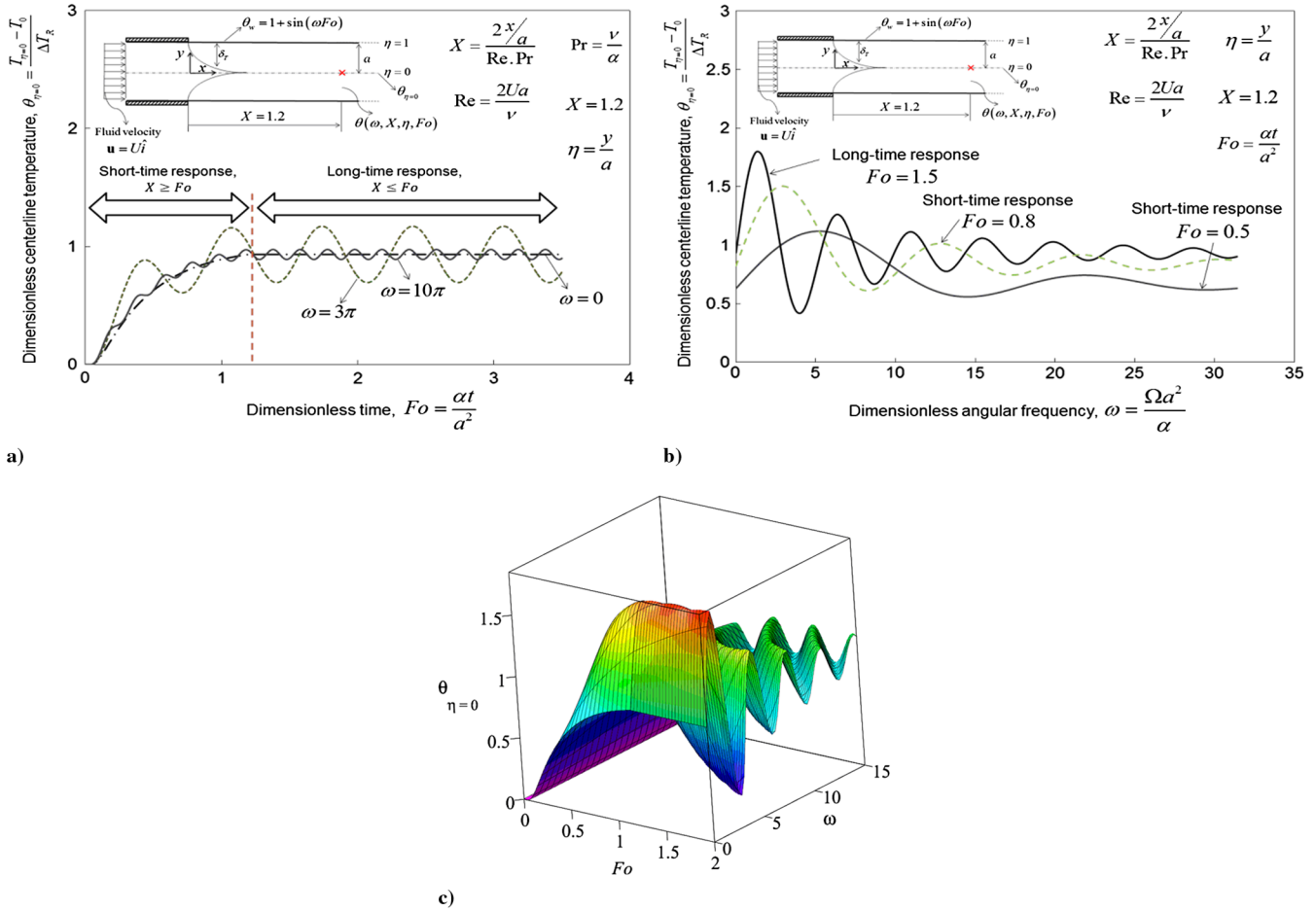

Fig. 5 Centerline temperature against: a) *Fo* number, b) angular frequency, and c) *Fo* and angular frequency.

2) When a sinusoidal cyclic wall temperature with high angular frequency is imposed on the flow, the fluid does not follow the details of the imposed temperature behavior. Therefore, for high angular frequencies, the flow acts as if the imposed temperature is constant at "the average value" associated with zero frequency [Eq. (11)] for the sinusoidal heat flux in this case, in mathematical terms $\theta_{\omega\to\infty}\approx\theta_{\omega\to 0}$.

3) A conventional way to decrease the temperature of the working fluid inside the heat exchangers is to cool down the surface temperature. However, it is shown that changing the surface temperature frequency can also dramatically alter the fluid temperature.

4) The highest temperature for the centerline temperature occurs for small values of angular frequency. Considering Eq. (12b), the highest long-time centerline temperature occurs at

$$\frac{\mathrm{d}\theta_{\eta=0}}{\mathrm{d}\omega}=0\Rightarrow\omega\approx\pi\ \text{(rad)} \tag{21}$$

At a given axial position, the maximum long-time centerline temperature is remarkably higher than that of the short-time response.

Figure 6 shows the variations of the dimensionless wall heat flux at a given arbitrary axial position of $X=1.2$ versus the Fourier number and the dimensionless angular frequency; Eqs. (16a) and (16b). In addition, a comparison is made between the exact series solutions [Eqs. (16a) and (16b)] and the developed compact relationships [Eqs. (20a) and (20b)]. As seen from Fig. 6, there is an excellent agreement between the exact solution and the compact relationships; the maximum relative difference less than 4.6%.

From Fig. 6, one can conclude the following:

1) The dimensionless wall heat flux oscillates with the angular frequency of the imposed wall temperature. This is indicated by the developed compact relationships; Eqs. (20a) and (20b).

2) The dimensionless wall heat flux oscillates around the step wall heat flux response. In other words, as $\omega\to 0$, the dimensionless wall heat flux yields the response of the step wall temperature condition.

3) Regardless of the angular frequency, at a very initial transient period, the dimensionless wall heat flux is much higher than that of the long-time response.

4) The amplitude of the dimensionless wall heat flux increases with the angular frequency of the imposed wall temperature. It should be noted that increasing the angular frequency does not affect the amplitude of the imposed wall temperature; see Eq. (9). However, as mentioned before, it decreases the amplitude of the fluid temperature toward the centerline. Therefore, as the angular frequency of the

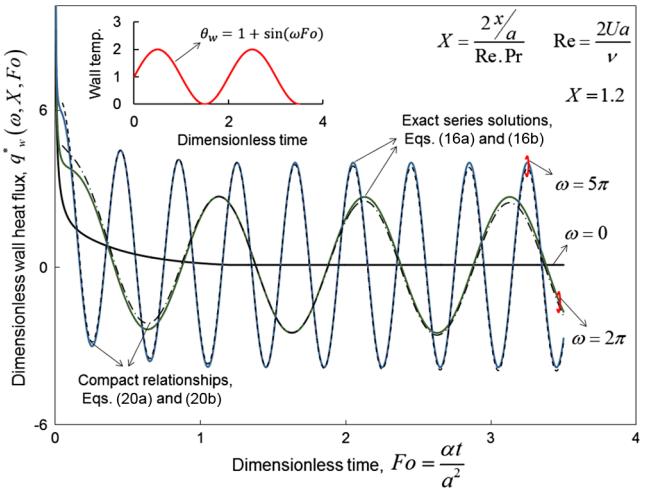

Fig. 6 Exact and approximate wall heat fluxes versus *Fo* number for different angular frequencies.

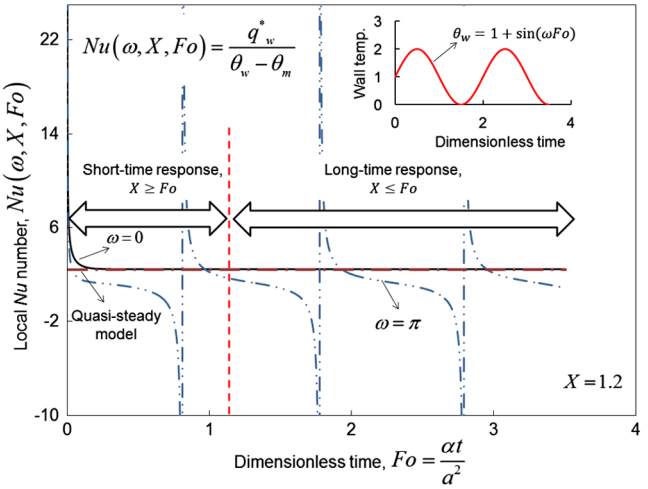

Fig. 7 Local Nu number against Fo number for different angular frequencies.

imposed temperature rises, the amplitude of the temperature gradient and heat flux in consequent increases.

5) The phase lag of the dimensionless wall heat flux is only a function of dimensionless angular frequency of the imposed wall temperature, as indicated by Eqs. (20a) and (20b), i.e.,

$$\Delta\varphi = \frac{-0.77\omega^2 - 23.45 \times \omega + 215.3}{\omega^2 - 30.51 \times \omega + 280.5}$$

As mentioned before, the dimensionless angular frequency is a function of temperature frequency, fluid thermophysical properties, and tube geometrical parameters.

Figure 7 shows the variations of the Nusselt number at a given arbitrary axial position of $X = 1.2$ versus the Fourier number for different angular frequencies; Eq. (17). In addition, the transient Nusselt number developed in this study [Eq. (17)] is compared with the conventional "quasi-steady" model, which is a simplified model assuming that the convective heat transfer coefficient is constant, equal to the fully developed condition in the channel [25].

The following can be concluded from Fig. 7:

1) The values of the transient Nusselt number deviate considerably from the ones predicted by the conventional quasi-steady model. Therefore, the conventional models fail to predict the transient Nusselt number accurately.

2) When $Fo \geq 0.2$, as the fluid flow becomes thermally fully developed, the presented model approaches the quasi-steady model for $\omega \to 0$, i.e., the step wall temperature condition.

3) The Nusselt number is positive when the heat flow is from the wall to the fluid, i.e., $\theta_w > \theta_m$. However, when the fluid bulk temperature is higher than the wall temperature, $\theta_m > \theta_w$, the Nusselt number is negative.

4) At some particular Fo numbers, the Nusselt number experiences discontinuities, soaring to plus infinity and then returning from minus infinity. These excursions occur when the wall and fluid bulk temperature are equal, $\theta_w = \theta_m$, but the heat flux is not zero; see Eq. (17). In fact, the Nusselt number loses its significance at such particular points. The same behavior for the Nusselt number was reported for the periodic inlet fluid temperature [40] and variable x-dependent wall temperature [41].

5) Comparing the results of this study with [40,41], when there is a periodic boundary condition for a convective duct flow, the temperature field inside the fluid fluctuates with the agitation angular frequency of the boundary.

6) Accordingly, we believe that the Nusselt number is not a proper candidate to represent the thermal characteristics of transient systems under harmonic prescribed temperature. Therefore, dimensionless wall heat flux can be considered as the best representative of the thermal behavior of a convective tube flow.

Figure 8 depicts the variations of the average dimensionless wall heat flux [Eq. (18)] against the dimensionless angular frequency and compared with the quasi-steady model. It should be noted that arbitrary intervals of axial positions are considered to calculate the integral in Eq. (18), i.e., $0 \leq X \leq 0.2$ and $0 \leq X \leq 1$. In addition, an arbitrary time interval of 0.8 is considered for the Fo number, $0 \leq Fo \leq 0.8$, over which the double integral in Eq. (18) is performed. Since the parameters are dimensionless, the same trend is observed for other arbitrarily chosen intervals of axial position X and Fo number.

One can conclude the following from Fig. 8:

1) The maximum average heat flux occurs at the dimensionless angular frequency of

$$\omega_{\text{opt.}} = \left(\frac{\Omega \times a^2}{\alpha}\right)_{\text{opt.}} = 2.4 \text{ rad}$$

2) Therefore, the optimum excitation angular frequency, Ω rad/s, is a function of the fluid properties and the geometrical parameters of the tube, $\Omega_{\text{opt.}} = 2.4 \times (\alpha/a^2)$ rad/s.

3) The values of the averaged wall heat flux vary significantly with the angular frequency of the imposed wall temperature, whereas the conventional models, e.g., quasi-steady model, fail to predict such variations of the dimensionless heat flux with time.

4) As an example for the optimum angular frequency, when $0 \leq X \leq 1$ and $0 \leq Fo \leq 0.8$, the value of the averaged dimensionless wall heat flux is almost 52% higher than the corresponding value for isothermal boundary condition (step wall temperature).

5) Regardless of the chosen intervals of Fo and X, the value of the optimum dimensionless angular frequency remains the same, $\omega_{\text{opt.}} = 2.4$ rad.

B. Arbitrary Time-Dependent Prescribed Temperature

In this section, a superposition technique is applied to the results for harmonic boundary condition, see Sec. VI.A. It is intended to obtain the temperature distribution inside a tube for an arbitrary time-dependent wall temperature and compare it with the numerical simulation data. The results presented here are dimensional; we believe this will provide one with a sense for the actual values of the discussed dimensionless variables of transient internal forced convection.

Consider a parallel plate with half-width $\alpha = 0.31$ cm, in which water is flowing at uniform velocity, $U = 2.4$ cm/s. The thermophysical properties of the working fluid and the geometrical parameters are previously presented in Table 2. The prescribed temperature is considered arbitrarily in the following general form:

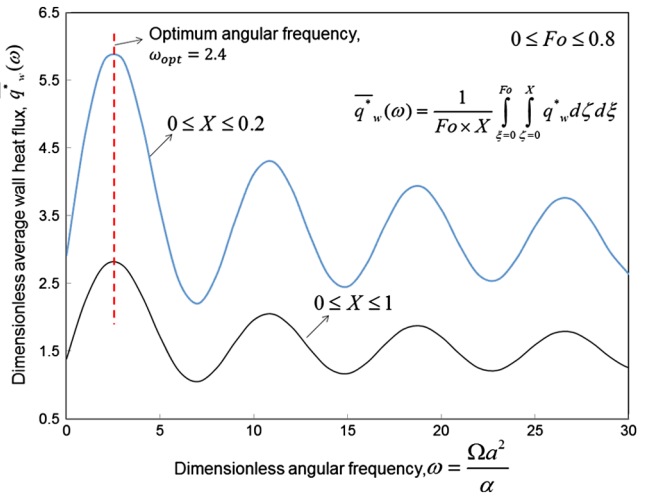

Fig. 8 Variations of the average dimensionless wall heat flux [Eq. (18)] with the angular frequency over arbitrarily chosen intervals of axial positions and Fo number.

Table 1 Summary of the literature regarding unsteady internal forced convection

Author	Velocity profile	Notes
Siegel [19]	Slug flow	Reported temperature distribution inside the fluid in Cartesian and cylindrical coordinates. Limited to step wall temperature/heat flux.
Siegel [20]	Poiseuille flow	Reported temperature distribution inside the fluid in cylindrical coordinate. Limited to step wall temperature condition.
Sparrow and Siegel [21,22]	Poiseuille flow	Reported tube wall temperature/heat flux. Limited to homogenous boundary conditions, i.e., step wall temperature/heat flux. Limited to thermal entrance region.
Perlmutter and Siegel [26]	Poiseuille flow	Evaluated tube wall temperature considering the wall thermal inertia. Limited to step wall temperature condition.
Sucec [27]	Slug flow	Evaluated fluid temperature under sinusoidal wall heat flux. Limited to quasi-steady assumption.

Table 2 Fluid properties and dimensions of the tube for the baseline case in numerical simulation[a]

Parameter	Value
Thermal conductivity k, W/m/k	0.64
Thermal diffusivity α, m^2/s	1.6E-7
Kinematic viscosity ν, m^2/s	5.66E-7
Tube half-width a, m	0.003
Tube length L, cm	250

[a] $Re_a = 100$.

Table 3 Parameters in Eq. (22)

Parameter	Value
T_0, K	300
Ω_1, rad/s	0.06
Ω_2, rad/s	0.12
Ω_3, rad/s	0.24
Ω_4, rad/s	0.1
$\Delta T_{R,1}$, K	1
$\Delta T_{R,2}$, K	4
$\Delta T_{R,3}$, K	10
$\Delta T_{R,4}$, K	8
T_1, K	5
T_2, K	10
T_3, K	15
T_4, K	20

$$T_w = T_0 + \sum_{i=1}^{4}[T_i + \Delta T_{R,i}\ \sin(\Omega_i t)] \tag{22}$$

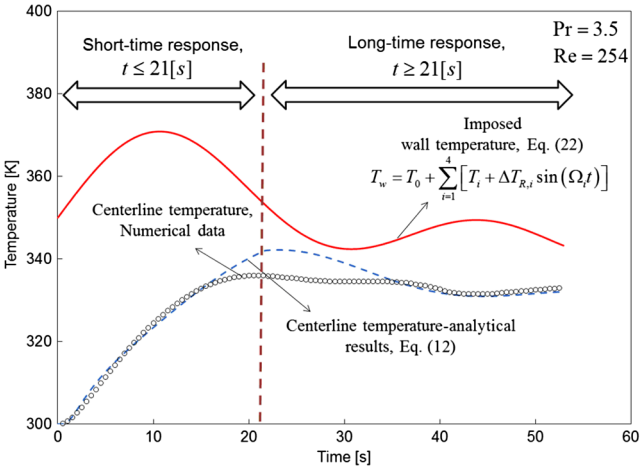

Fig. 9 Centerline temperature [Eq. (11)] versus time, and comparison with the obtained numerical data for a general boundary condition [Eq. (20)].

The parameters in Eq. (22) are introduced in Table 3. It should be noted that T_0 is the initial temperature of the fluid, and T_i and $\Delta T_{R,i}$ are the constant values and the amplitudes of the imposed wall temperature, respectively. The values for the parameters in Eq. (22) are arbitrarily chosen, and a similar approach can be taken for other forms of time-dependent boundary conditions.

Figure 9 displays the transient centerline temperature, at an arbitrarily chosen axial position, $x = 50$ cm, under a time-dependent wall temperature [Eq. (22)] in comparison with the obtained numerical data. The imposed wall temperature is also depicted in Fig. 9 by a solid line. The markers in Fig. 9 are the numerical data, and the solid lines are the analytical results. There is a good agreement between the analytical results and the numerical simulation data; the maximum relative difference is less than 5%.

The following can be concluded from Fig. 9:

1) The short-time response, $t \le 21$ s, at which pure conduction heat transfer occurs is much lower than the long time response, $t \ge 21$ s.

2) The presented model can be applied to find the fluid temperature inside a tube under any type of arbitrary time-dependent wall temperature.

3) The maximum discrepancy between the analytical results and the obtained numerical data occurs around the transition time, as stated for the trends in Fig. 3. This occurs since the analytical model predicts an abrupt arrival from short-time to long-time response, whereas the numerical simulation predicts a smooth transition; see [19] for more detail.

VII. Conclusions

A new full-time-range analytical model is developed to predict the transient thermal performance of forced-convective tube flow under an arbitrary time-dependent wall temperature. The methodology is presented in Cartesian and cylindrical coordinates. The slug flow condition is considered for the velocity distribution inside a circular tube. As such, new all-time models are developed to evaluate 1) temperature distribution inside the fluid; 2) fluid bulk temperature; 3) dimensionless wall heat flux; and 4) Nusselt number. Furthermore, compact closed-form relationships are proposed to predict such thermal characteristics of the tube flow with the maximum relative difference of less than 10%. A new heat transfer enhancement technique is presented for convective tube flow under harmonic boundary temperature. Optimizing the angular frequency of the imposed wall temperature can remarkably increase the overall heat transfer rate of a convective tube flow. The analytical results are verified successfully with the obtained numerical data. The maximum relative difference between the analytical results and the numerical data is less than 4.9%. The highlights of the present study can be listed as follows:

1) There is a thermal lag in the thermal response of the fluid temperature that increases toward the centerline of the tube due to the thermal inertia of the fluid.

2) The fluid temperature, dimensionless wall heat flux, and Nusselt number oscillate with the angular frequency of the imposed wall temperature.

3) At the two limiting cases, the thermal response of the fluid yields that of the step wall temperature: 1) $\omega \to 0$ and 2) $\omega \to \infty$.

4) There is an optimum value for the dimensionless angular frequency of the imposed harmonic wall temperature that maximizes the average dimensionless wall heat flux:

$$\omega_{\text{opt.}} = \left(\frac{\Omega \times a^2}{\alpha}\right)_{\text{opt.}} = 2.43 \text{ rad}$$

Acknowledgments

This work was supported by Automotive Partnership Canada, grant no. APCPJ 401826-10. The authors would like to thank the support of the industry partner Future Vehicle Technologies, Inc. (British Columbia, Canada).

References

[1] Agyenim, F., Hewitt, N., Eames, P., and Smyth, M., "A Review of Materials, Heat Transfer and Phase Change Problem Formulation for Latent Heat Thermal Energy Storage Systems (Lhtess)," *Renewable and Sustainable Energy Reviews*, Vol. 14, No. 2, Feb. 2010, pp. 615–628. doi:10.1016/j.rser.2009.10.015

[2] Cabeza, L. F., Mehling, H., Hiebler, S., and Ziegler, F., "Heat Transfer Enhancement in Water when Used as PCM in Thermal Energy Storage," *Applied Thermal Engineering*, Vol. 22, No. 10, July 2002, pp. 1141–1151. doi:10.1016/S1359-4311(02)00035-2

[3] Kurklo, A., "Energy Storage Applications in Greenhouses by Means of Phase Change Materials (PCMs): A Review," *Renewable Energy*, Vol. 13, No. 1, 1998, pp. 89–103. doi:10.1016/S0960-1481(97)83337-X

[4] Garrison, J. B., and Webber, E. M., "Optimization of an Integrated Energy Storage for a Dispatchable Wind Powered Energy System," *ASME 2012 6th International Conference on Energy Sustainability*, American Soc. of Mechanical Engineers, Fairfield, NJ, 2012, pp. 1–11.

[5] Sawin, J. L., and Martinot, E., "Renewables Bounced Back in 2010, Finds REN21 Global Report," *Renewable Energy World*, 2011, Data available online at http://www.renewableenergyworld.com/rea/news/article/2011/09/renewables-bounced-back-in-2010-finds-ren21-global-report [retrieved 2014].

[6] Bennion, K., and Thornton, M., "Integrated Vehicle Thermal Management for Advanced Vehicle Propulsion Technologies," National Renewable Energy Lab. NREL/CP-540-47416, Golden, CO, 2010.

[7] Boglietti, A., Member, S., Cavagnino, A., Staton, D., Shanel, M., Mueller, M., and Mejuto, C., "Evolution and Modern Approaches for Thermal Analysis of Electrical Machines," *IEEE Transactions on Industrial Electronics*, Vol. 56, No. 3, 2009, pp. 871–882. doi:10.1109/TIE.2008.2011622

[8] Canders, W.-R., Tareilus, G., Koch, I., and May, H., "New Design and Control Aspects for Electric Vehicle Drives," *2010 14th International Power Electronics and Motion Control Conference (EPE/PEMC)*, IEEE Xplore, Sept. 2010, pp. S11-1, S11-8. doi:10.1109/EPEPEMC.2010.5606528

[9] Hamada, K., "Present Status and Future Prospects for Electronics in Electric Vehicles/Hybrid Electric Vehicles and Expectations for Wide Bandgap Semiconductor Devices," *Physica Status Solidi (B)*, Vol. 245, No. 7, July 2008, pp. 1223–1231. doi:10.1002/pssb.v245:7

[10] Hale, M., "Survey of Thermal Storage for Parabolic Trough Power Plants," National Renewable Energy Lab. NREL/SR-550-27925, Golden, CO, 2000, pp. 1–28.

[11] Sharma, A., Tyagi, V. V., Chen, C. R., and Buddhi, D., "Review on Thermal Energy Storage with Phase Change Materials and Applications," *Renewable and Sustainable Energy Reviews*, Vol. 13, No. 2, Feb. 2009, pp. 318–345. doi:10.1016/j.rser.2007.10.005

[12] März, M., Schletz, A., Eckardt, B., Egelkraut, S., and Rauh, H., "Power Electronics System Integration for Electric and Hybrid Vehicles," *Integrated Power Electronics Systems (CIPS)*, IEEE Xplore, March 2010, pp. 1–10, 16–18, Data available online at http://ieeexplore.ieee.org/stamp/stamp.jsp?tp=&=5730643&=5730626.

[13] Nerg, J., Rilla, M., and Pyrhönen, J., "Thermal Analysis of Radial-Flux Electrical Machines with a High Power Density," *IEEE Transactions on Industrial Electronics*, Vol. 55, No. 10, 2008, pp. 3543–3554. doi:10.1109/TIE.2008.927403

[14] "Cumulative Sales of TMC Hybrids Top 2 Million Units in Japan," Toyota Motor Corporation, Japan, 2012, Data available online at http://www.toyotabharat.com/inen/news/2013/april_17.aspx [retrieved 2014].

[15] O'Keefe, M., and Bennion, K., "A Comparison of Hybrid Electric Vehicle Power Electronics Cooling Options," *IEEE Vehicle Power and Propulsion Conference (VPPC)*, IEEE Xplore, 2007, pp. 116–123, 9–12. doi:10.1109/VPPC.2007.4544110

[16] Bennion, K., and Thornton, M., "Integrated Vehicle Thermal Management for Advanced Vehicle Propulsion Technologies," National Renewable Energy Lab. NREL/CP-540-47416, Golden, CO, 2010.

[17] Johnson, R. W., Evans, J. L., Jacobsen, P., Thompson, J. R. R., and Christopher, M., "The Changing Automotive Environment: High-Temperature Electronics," *IEEE Transactions on Electronics Packaging Manufacturing*, Vol. 27, No. 3, July 2004, pp. 164–176. doi:10.1109/TEPM.2004.843109

[18] Kelly, K., Abraham, T., and Bennion, K., "Assessment of Thermal Control Technologies for Cooling Electric Vehicle Power Electronics," National Renewable Energy Lab. NREL/CP-540-42267, Golden, CO, 2008.

[19] Siegel, R., "Transient Heat Transfer for Laminar Slug Flow in Ducts," *Applied Mechanics*, Vol. 81, No. 1, 1959, pp. 140–144.

[20] Siegel, R., "Heat Transfer for Laminar Flow in Ducts with Arbitrary Time Variations in Wall Temperature," *Journal of Applied Mechanics*, Vol. 27, No. 2, 1960, pp. 241–249. doi:10.1115/1.3643945

[21] Sparrow, E. M., and Siegel, R., "Thermal Entrance Region of a Circular Tube Under Transient Heating Conditions," *Third U.S. National Congress of Applied Mechanics*, ASME Trans., 1958, pp. 817–826.

[22] Siegel, R., and Sparrow, E. M., "Transient Heat Transfer for Laminar Forced Convection in the Thermal Entrance Region of Flat Ducts," *ASME Heat Transfer*, Vol. 81, No. 1, 1959, pp. 29–36.

[23] Perlmutter, M., and Siegel, R., "Unsteady Laminar Flow in a Duct with Unsteady Heat Addition," *Heat Transfer*, Vol. 83, No. 4, 1961, pp. 432–439. doi:10.1115/1.3683662

[24] Siegel, R., "Forced Convection in a Channel with Wall Heat Capacity and with Wall Heating Variable with Axial Position and Time," *International Journal of Heat Mass Transfer*, Vol. 6, No. 7, 1963, pp. 607–620. doi:10.1016/0017-9310(63)90016-4

[25] Siegel, R., and Perlmutter, M., "Laminar Heat Transfer in a Channel with Unsteady Flow and Wall Heating Varying with Position and Time," *Journal of Heat Transfer*, Vol. 85, No. 4, 1963, pp. 358–365. doi:10.1115/1.3686125

[26] Perlmutter, M., and Siegel, R., "Two-Dimensional Unsteady Incompressible Laminar Duct Flow with a Step Change in Wall Temperature," *Journal of Heat Transfer*, Vol. 83, No. 4, 1961, pp. 432–440. doi:10.1115/1.3683662

[27] Sucec, J., "Unsteady Forced Convection with Sinusoidal Duct Wall Generation: The Conjugate Heat Transfer Problem," *International Journal of Heat and Mass Transfer*, Vol. 45, No. 8, April 2002, pp. 1631–1642. doi:10.1016/S0017-9310(01)00275-7

[28] Kakac, S., Li, W., and Cotta, R. M., "Unsteady Laminar Forced Convection in Ducts with Periodic Variation of Inlet Temperature," *Heat Transfer*, Vol. 112, No. 4, 1990, pp. 913–920. doi:10.1115/1.2910499

[29] Weigong, L., and Kakac, S., "Unsteady Thermal Entrance Heat Transfer in Laminar Flow with a Periodic Variation of Inlet Temperature," *International Journal of Heat and Mass Transfer*, Vol. 34, No. 10, Oct. 1991, pp. 2581–2592. doi:10.1016/0017-9310(91)90098-Y

[30] Kakac, S., and Yener, Y., "Exact Solution of the Transient Forced Convection Energy Equation for Timewise Variation of Inlet Temperature," *International Journal of Heat Mass Transfer*, Vol. 16, No. 12, 1973, pp. 2205–2214. doi:10.1016/0017-9310(73)90007-0

[31] Cotta, R. M., and Özişik, M. N., "Laminar Forced Convection Inside Ducts with Periodic Variation of Inlet Temperature," *International Journal of Heat and Mass Transfer*, Vol. 29, Oct. 1986, pp. 1495–1501. doi:10.1016/0017-9310(86)90064-5

[32] Kakac, S., "A General Analytical Solution to the Equation of Transient Forced Convection with Fully Developed Flow," *International Journal of Heat Mass Transfer*, Vol. 18, No. 12, 1975, pp. 1449–1454. doi:10.1016/0017-9310(75)90259-8

[33] Hadiouche, A., and Mansouri, K., "Application of Integral Transform Technique to the Transient Laminar Flow Heat Transfer in the Ducts," *International Journal of Thermal Sciences*, Vol. 49, No. 1, Jan. 2010, pp. 10–22. doi:10.1016/j.ijthermalsci.2009.05.012

[34] Fakoor-Pakdaman, M., Andisheh-Tadbir, M., and Bahrami, M., "Transient Internal Forced Convection Under Arbitrary Time-Dependent Heat Flux," *Proceedings of the ASME 2013 Summer Heat Transfer Conference HT2013*, ASME-17148, Minneapolis, MN, 2013.
[35] Fakoor-Pakdaman, M., Andisheh-Tadbir, M., and Bahrami, M., "Unsteady Laminar Forced-Convective Tube Flow Under Dynamic Time-Dependent Heat Flux," *Journal of Heat Transfer*, Vol. 136, No. 4, Nov. 2013, Paper 041706. doi:10.1115/1.4026119
[36] Kreyszig, E., Kreyzig, H., and Norminton, E. J., *Advanced Engineering Methematics*, Wiley, New York, 2010, pp. 473–490.
[37] Campo, A., Morrone, B., and Manca, O., "Approximate Analytic Estimate of Axial Fluid Conduction in Laminar Forced Convection Tube Flows with Zero-to-Uniform Step Wall Heat Fluxes," *Heat Transfer Engineering*, Vol. 24, No. 4, July 2003, pp. 49–58. doi:10.1080/01457630304027
[38] Incropera, F. P., Dewitt, D. P., Bergman, T. L., and Lavine, A. S., *Introduction to Heat Transfer*, Wiley, New York, 2007, p. 458.
[39] Bejan, A., *Convection Heat Transfer*, Wiley, New York, 2004, p. 119.
[40] Sparrow, E. M., and Farias, F. N. De., "Unsteady Heat Transfer in Ducts With Time-Varying Inlet Tempearture and Participating Walls," *International Journal of Heat Mass Transfer*, Vol. 11, No. 5, 1968, pp. 837–853. doi:10.1016/0017-9310(68)90128-2
[41] Kays, W. M., and Crawford, M. E., *Convective Heat and Mass Transfer*, McGraw–Hill, New York, 1993, pp. 140–146.